Supporting Information

Increasing Heat Transfer Performance of Thermoplastic Polyurethane by Constructing Thermal Conduction Channels of Ultra-thin Boron Nitride Nanosheets and Carbon Nanotubes

Yue Ruan,[a, b] Nian Li,[a, c] Cui Liu,[a, c] Liqing Chen,[a, b] Shudong Zhang,[a, c,] Zhenyang Wang[a,c,*]*

[†]Institute of Solid State Physics, Hefei Institutes of Physical Science, Chinese Academy of Sciences, Hefei, Anhui 230031, China

[‡]Department of Chemistry, University of Science and Technology of China, Hefei, Anhui 230026, China

[#]Key Laboratory of Photovoltaic and Energy Conservation Materials, Hefei Institutes of Physical Science, Chinese Academy of Sciences, Hefei 230031, China

[*]Corresponding Author

E-mail: zywang@iim.ac.cn, sdzhang@iim.ac.cn

KEYWORDS: h-BNNSs; CNTs; TPU; TIMs; multi-path; thermal conductivity

Table of Contents

Figure S1 **S-3**

Mechanism diagram of h-BNNSs exfoliation starting from the bulk h-BN.

Figure S2 **S-3**

The comparison of solubility between h-BN and h-BNNSs**.**

Figure S3 **S-3**

The comparison of Tyndall phenomenon between h-BN and h-BNNSs.

Figure S4 **S-4**

Morphological characteristics of h-BNNSs after exfoliation. (a) Low magnification TEM images of exfoliated h-BNNSs obtained by hydrothermal exfoliation method; (b) TEM image of the edge of h-BNNSs; (c) HRTEM image of the h-BNNSs with the clear lattice fringes; (d) A representative SAED pattern of h-BNNSs; (e) AFM topography image of h-BNNSs; (f) Cross-sectional analysis diagram of h-BNNSs.

Figure S5 **S-4**

Elongation at break of h-BNNSs/CNTs/TPU composites with different TPU contents. ε is elongation at break; L is the original length of the sample and ΔL is the difference between the stretched length and the original length.

Figure S6 **S-5**

The XRD patterns of the h-BN and h-BNNSs.

Figure S7 **S-5**

The XRD patterns of the CNTs before and after acidification.

Figure S8 **S-5**

XRD patterns of h-BNNSs, TPU, CNTs and the h-BNNSs/CNTs/TPU composite membrane.

Figure S9 **S-6**

FTIR spectra of h-BNNSs, CNTs, TPU and the h-BNNSs/CNTs/TPU composite membrane.

Figure S10 **S-6**

FTIR spectra of h-BNNSs and the h-BNNSs/CNTs/TPU composite.

Figure S11 **S-7**

FTIR spectra of TPU and the h-BNNSs/CNTs/TPU composite membrane.

Figure S12 **S-7**

FTIR spectra of CNTs before and after acidification.

Figure S13 **S-7**

Thermogravimetric analysis curves of h-BNNSs/CNTs/TPU composite membrane with different mass fractions of TPU.

Figure S14 **S-8**

Thermogravimetric analysis curves of h-BNNSs and CNTs.

Figure S15 **S-8**

Thermal conductivity enhancements and thermal diffusivity enhancements of h-BNNSs/CNTs/TPU composite membrane with different h-$BNNS_X$/CNT_Y content ratio via transverse measurement.

Figure S16 **S-8**

Thermal conductivity and thermal diffusivity of h-BNNSs/CNTs/TPU composite membrane with different content ratio of h-$BNNS_X$/CNT_Y by lateral measurement.

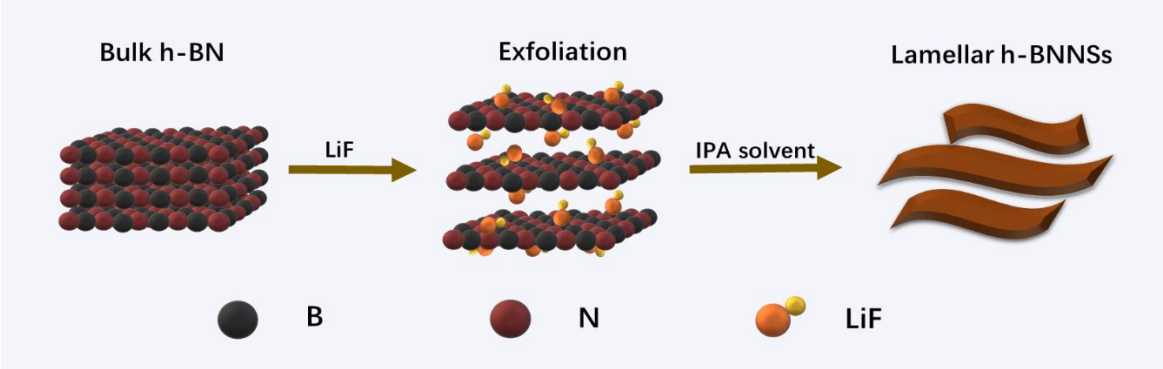

Figure S1. Mechanism diagram of h-BNNSs exfoliation starting from the bulk h-BN.

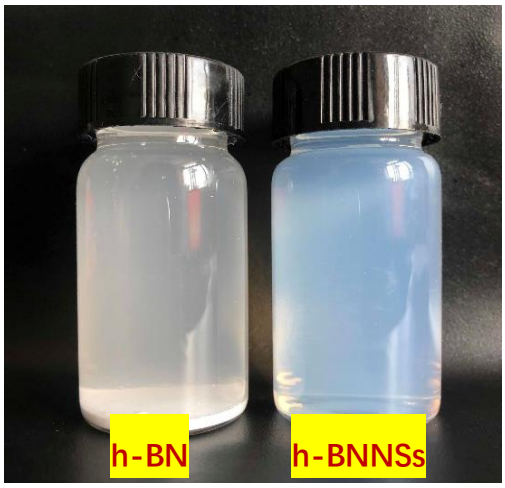

Figure S2. The comparison of solubility between h-BN and h-BNNSs**.**

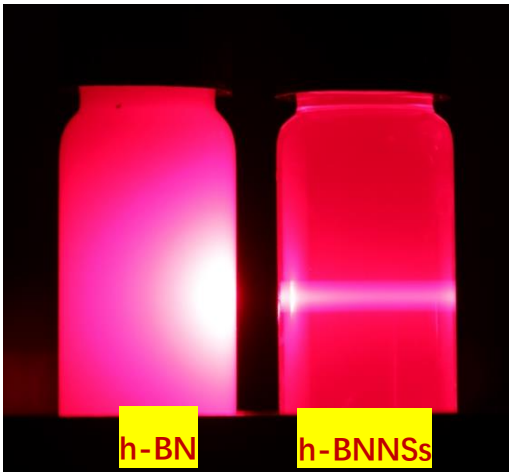

Figure S3. The comparison of Tyndall phenomenon between h-BN and h-BNNSs.

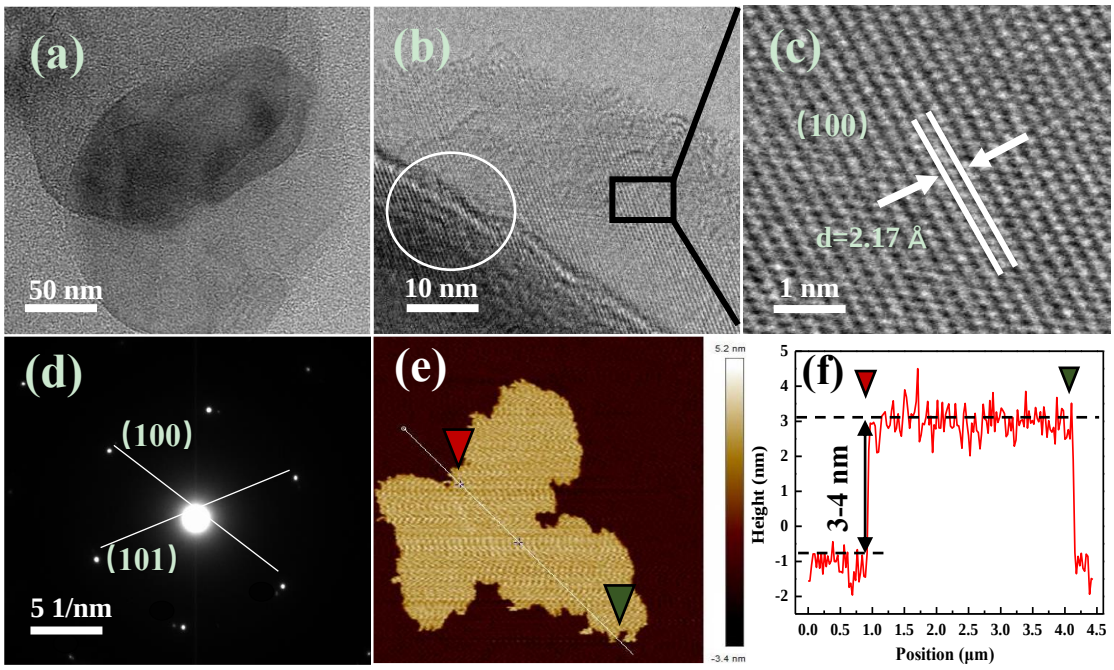

Figure S4. Morphological characteristics of h-BNNSs after exfoliation. (a) Low magnification TEM images of exfoliated h-BNNSs obtained by hydrothermal exfoliation method; (b) TEM image of the edge of h-BNNSs; (c) HRTEM image of the h-BNNSs with the clear lattice fringes; (d) A representative SAED pattern of h-BNNSs; (e) AFM topography image of h-BNNSs; (f) Cross-sectional analysis diagram of h-BNNSs.

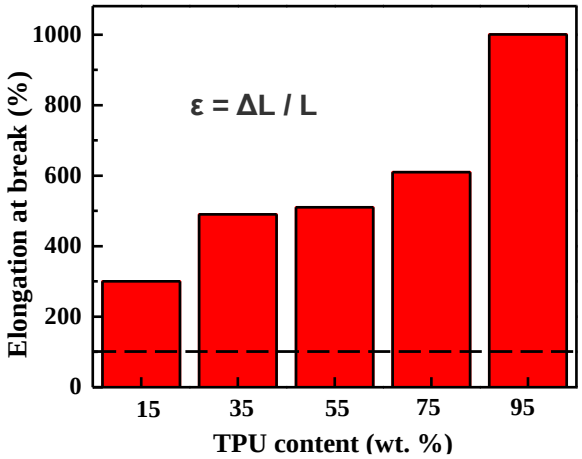

Figure S5. Elongation at break of h-BNNSs/CNTs/TPU composites with different TPU contents. ε is elongation at break; L is the original length of the sample and ΔL is the difference between the stretched length and the original length.

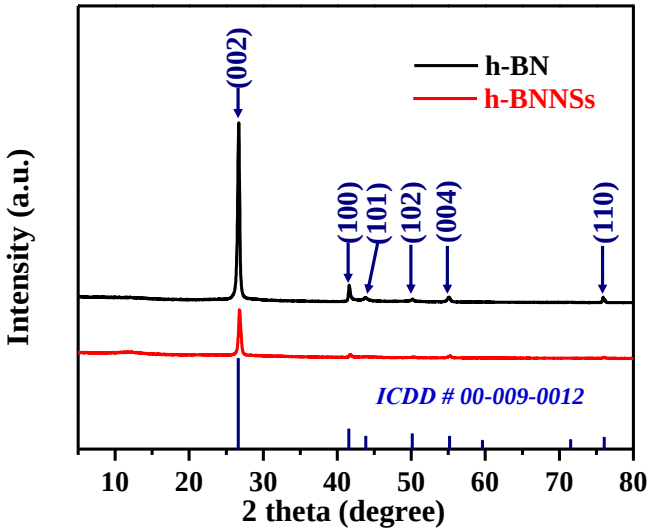

Figure S6. The XRD patterns of the h-BN and h-BNNSs.

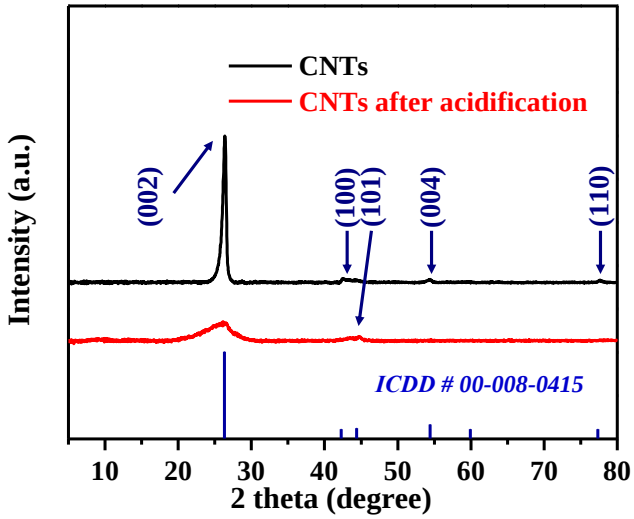

Figure S7. The XRD patterns of the CNTs before and after acidification.

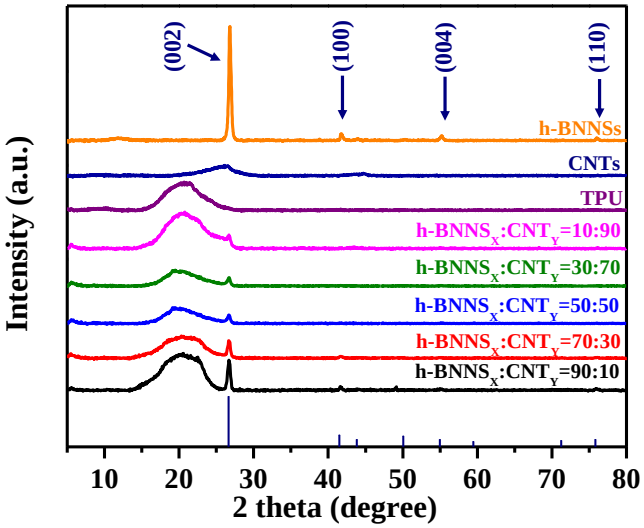

Figure S8. XRD patterns of h-BNNSs, TPU, CNTs and the h-BNNSs/CNTs/TPU

composite membrane with different h-BNNS$_X$/CNT$_Y$ content ratio.

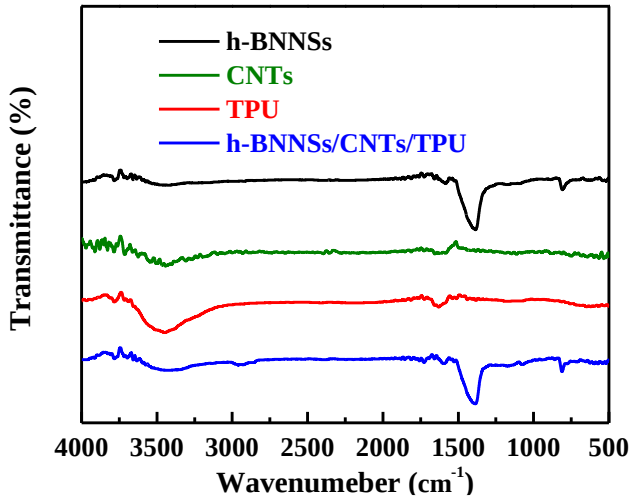

Figure S9. FTIR spectra of h-BNNSs, CNTs, TPU and the h-BNNSs/CNTs/TPU composite membrane.

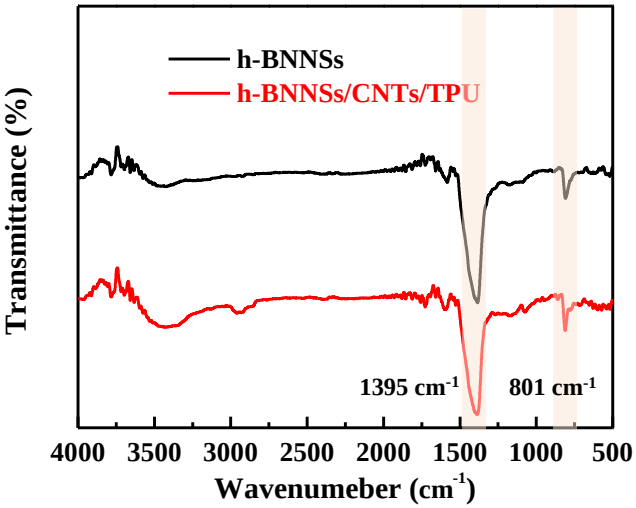

Figure S10. FTIR spectra of h-BNNSs and the h-BNNSs/CNTs/TPU composite membrane.

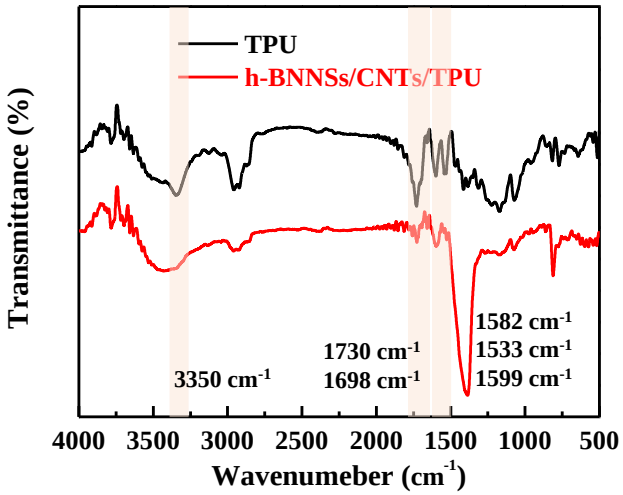

Figure S11. FTIR spectra of TPU and the h-BNNSs/CNTs/TPU composite. membrane.

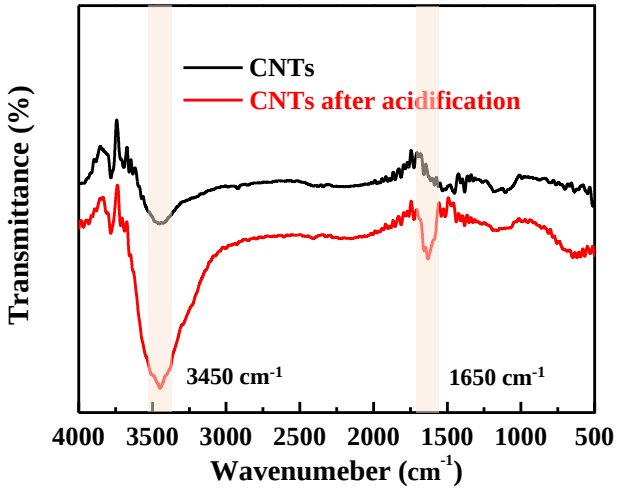

Figure S12. FTIR spectra of CNTs before and after acidification.

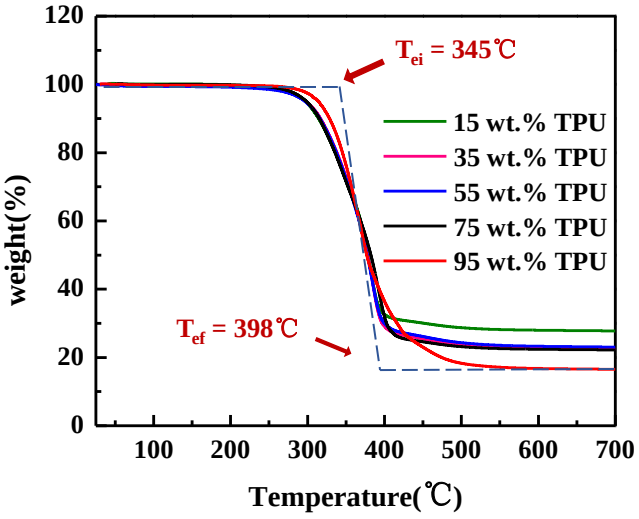

Figure S13. Thermogravimetric analysis curves of h-BNNSs/CNTs/TPU composite membrane with different mass fractions of TPU.

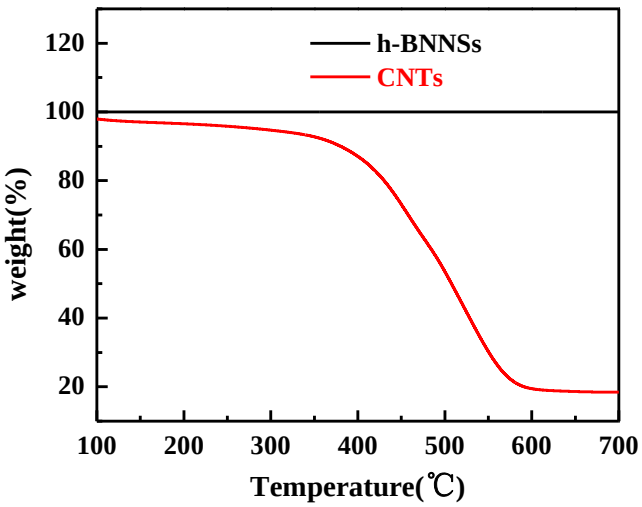

Figure S14. Thermogravimetric analysis curves of h-BNNSs and CNTs.

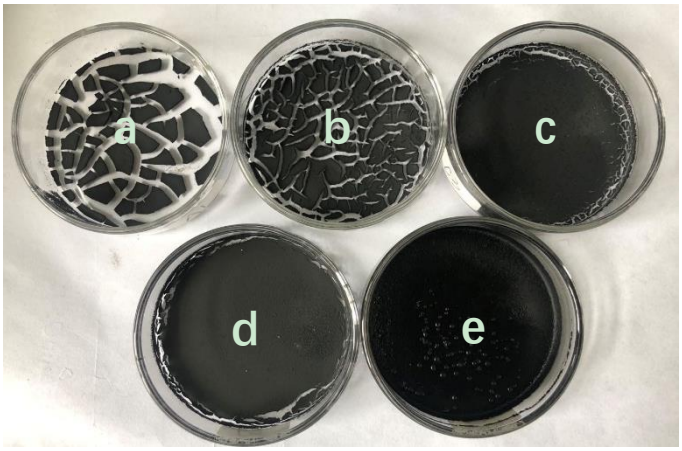

Figure S15. Five types of h-BNNSs/CNTs/TPU composite membrane with TPU content of (a) 15 wt.%; (b) 20 wt.%; (c) 25 wt.%; (d) 30 wt.%; and (e) 35 wt.%, respectively.

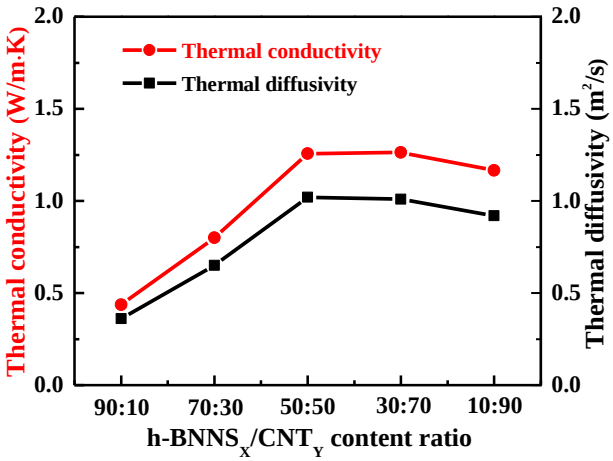

Figure S16. Thermal conductivity and thermal diffusivity of h-BNNSs/CNTs/TPU composite membrane with different content ratio of h-$BNNS_X$/CNT_Y by lateral

measurement.